THE ASTROPHYSICAL JOURNAL, 411:802–812, 1993 July 10

ON THE MASS OF THE COMPACT OBJECT IN THE BLACK HOLE BINARY A0620−00

CAROLE A. HASWELL[1] AND EDWARD L. ROBINSON
McDonald Observatory and Department of Astronomy, University of Texas, Austin, TX 78712
KEITH HORNE[2]
Space Telescope Science Institute, 3700 San Martin Drive, Baltimore, MD 21218
RAE F. STIENING[2]
Superconducting Super Collider Laboratory, 2550 Beckleymeade Avenue, MS 1090, Dallas, TX 75237
AND
TIMOTHY M. C. ABBOTT
McDonald Observatory and Department of Astronomy, University of Texas, Austin, TX 78712
Received 1992 November 11; accepted 1993 January 19

ABSTRACT

Multicolor orbital light curves of the black hole candidate binary A0620−00 are presented. The light curves exhibit ellipsoidal variations and a grazing eclipse of the mass donor companion star by the accretion disk. Synthetic light curves were generated using realistic mass donor star fluxes and an isothermal blackbody disk. For mass ratios of $q = M_1/M_2 = 5.0$, 10.6, and 15.0 systematic searches were executed in parameter space for synthetic light curves that fit the observations. For each mass ratio, acceptable fits were found only for a small range of orbital inclinations. It is argued that the mass ratio is unlikely to exceed $q = 10.6$, and an upper limit of $0.8M_\odot$ is placed on the mass of the companion star. These constraints imply $4.16 \pm 0.1M_\odot \leq M_1 \leq 5.55 \pm 0.15\ M_\odot$. The lower limit on M_1 is more than 4 σ above the mass of a maximally rotating neutron star and constitutes further strong evidence in favor of a black hole primary in this system.

Subject headings: binaries: close — black hole physics — stars: individual: (A0620−00)

1. INTRODUCTION

The X-ray nova A0620−00 (Nova Mon 1917, 1975), discovered by the *Ariel V* sky survey experiment (Elvis et al. 1975), is an interacting binary star with a K dwarf star transferring mass to an accretion disk around a compact primary star (Whelan et al. 1977; Oke 1977). McClintock & Remillard (1986) showed that the orbital period of A0620−00 is $P = 7.75234 \pm 0.00010$ hr, and that the radial velocity variation of the K dwarf component has a semiamplitude, K_2, of 457 ± 8 km s^{-1}. The orbital period and K velocity yield a mass function (which is the absolute lower limit on the compact object mass) of $f(M_1) = 3.19 \pm 0.17\ M_\odot$. Subsequent observations have refined this result and the current preferred mass function is $2.91 \pm 0.08\ M_\odot$ (Johnston, Kulkarni, & Oke 1989; McClintock 1992). The most widely accepted upper bound on the gravitational mass of a nonrotating neutron star is $3.2\ M_\odot$, based on the work of Rhoades & Ruffini (1974). Using Friedman & Ipser's (1987) approximate formula, and demanding that causality be obeyed, leads to an upper bound on the mass of a maximally rotating neutron star of $3.76\ M_\odot$. Thus the mass function of the compact object in A0620−00 established it as a strong black hole candidate. If the presence of a neutron star primary is to be ruled out, however, the constraints on the mass of the compact object in A0620−00 need to be improved.

The lower limit on M_1 can be translated into a true determination of M_1 if the orbital inclination, i, and the mass ratio, $q = M_1/M_2$, are known. A previous paper (Haswell & Shafter 1990) reported work addressing the mass ratio, q. Orbital variations in the radial velocity of the Hα emission line were detected. If these variations are attributed to the orbital motion of the compact object, the semiamplitude $K_1 = 43 \pm 8$ km s^{-1}. However, the phasing of the variations differs by $\sim 60°$ from that expected for the compact object radial velocity curve, so the interpretation is complicated. The deduced semiamplitude should be considered a plausible best estimate. Here we aim to constrain the orbital inclination, i. The light curves presented by McClintock & Remillard (1986) exhibit the so-called "ellipsoidal" variation, a double-humped variation caused by the changing projected area of the nonspherical secondary star as it proceeds around its orbit. The size of the ellipsoidal variation is dependent on the orbital inclination, and hence the orbital light curves can be used to deduce the inclination, i.

In § 2 we present multicolor orbital light curves of A0620−00; and in § 3 the results of computer modeling of these light curves are described. The resulting dynamical mass determination is elaborated in § 4. A compelling case for the elimination of the possibility of a neutron star primary in A0620−00 is presented.

2. OBSERVATIONS

A0620−00 was observed using the 2.7 m telescope at McDonald Observatory and the Stiening multicolor photometer, on the nights of 1986 December 27, 30, and 31, and 1987 January 1 and 2. The photometer accumulates data simultaneously in the U, B, V, and R bands on the program star; Horne & Stiening (1985) show the filter passbands. An integration time of 1 s was used in all observations. To facilitate accurate sky subtraction, the telescope was "nodded" under computer control between "star + sky" and "sky" continuously throughout the night, spending 30 s in each position. A nearby comparison star was monitored every 20–30 minutes; observations of flux standards were also obtained.

[1] Current address: Space Telescope Science Institute, 3700 San Martin Drive, Baltimore, MD 21218.
[2] Guest Observer, McDonald Observatory.

The data were reduced using DRAGON, an interactive analysis program for reduction of simultaneous multicolor photometry. Extraction of the U, B, and V data was made possible only by the simultaneous R-band data, in which the difference between "star" and "star + sky" was large enough to allow discrimination. Sky subtraction was performed by fitting a spline function to the series of sky measurements using χ^2 minimization. The comparison star observations were used to determine the extinction coefficients for each run, and the standard star observations calibrated the sensitivity of the instrument. Using the photometric ephemeris of McClintock & Remillard (1986), the flux-calibrated data were folded in orbital phase space to produce a mean orbital light curve in each color.

All the available data for A0620−00 are consistent with the predictions of the orbital ephemeris of McClintock & Remillard (1986): the photometric minima in the light curves herein and in Haswell et al. (1993, hereafter Paper II) occur at phases 0.0 and 0.5 to within the measurement errors. The orbital phase of the system has twice been unambiguously determined by measurements of the radial velocity curve of the late-type star (McClintock & Remillard 1986; Johnston et al. 1989); these observations rule out the possibility of a 1 yr alias causing a misidentification of phase 0.0 on alternate years. It is difficult to imagine that an alternative alias would produce such good fits to all the photometry: the photometric baseline is now almost a decade. Therefore we are confident that the phasing of our light curves is correct.

The quality of the data varied significantly from night to night, so a weighting scheme was used to average the data. Weights were assigned to 100 s segments of data by calculating the standard deviation of the data points in the segment. For ease of interpretation the data were subsequently rebinned into 50 orbital phase bins.

The flux-calibrated mean light curves are shown in Figure 1. The x-axes give orbital phase according to the standard convention: phase 0.0 corresponds to superior conjunction of the compact object. The ephemeris of McClintock & Remillard is 180° out of phase with this definition, since they adopted the deepest minimum in the orbital light curve as phase 0. The error bars in Figure 1 represent $\pm 1\ \sigma$ errors calculated from the point-to-point deviations in the light curves before rebinning. They do not include systematic errors or uncertainties in sky subtraction. These data were previously published in Haswell, Robinson, & Horne (1990); subsequent rereduction of the data uncovered an error in the recorded start time for the data taken on the night of 1986 December 31 (UT). This error was rectified, leading to a slight change in the shapes of the light curves.

The orbital modulations are pronounced and well defined in the B, V, and R light curves and present in the noisier U light curve. The dominant feature in the B, V, and R light curves is the double hump due to the ellipsoidal variation. The two ellipsoidal maxima are strongly asymmetric: the maximum preceding phase 0.5 is ~10% higher than the maximum following phase 0.5. A similar effect is apparent in the photometry

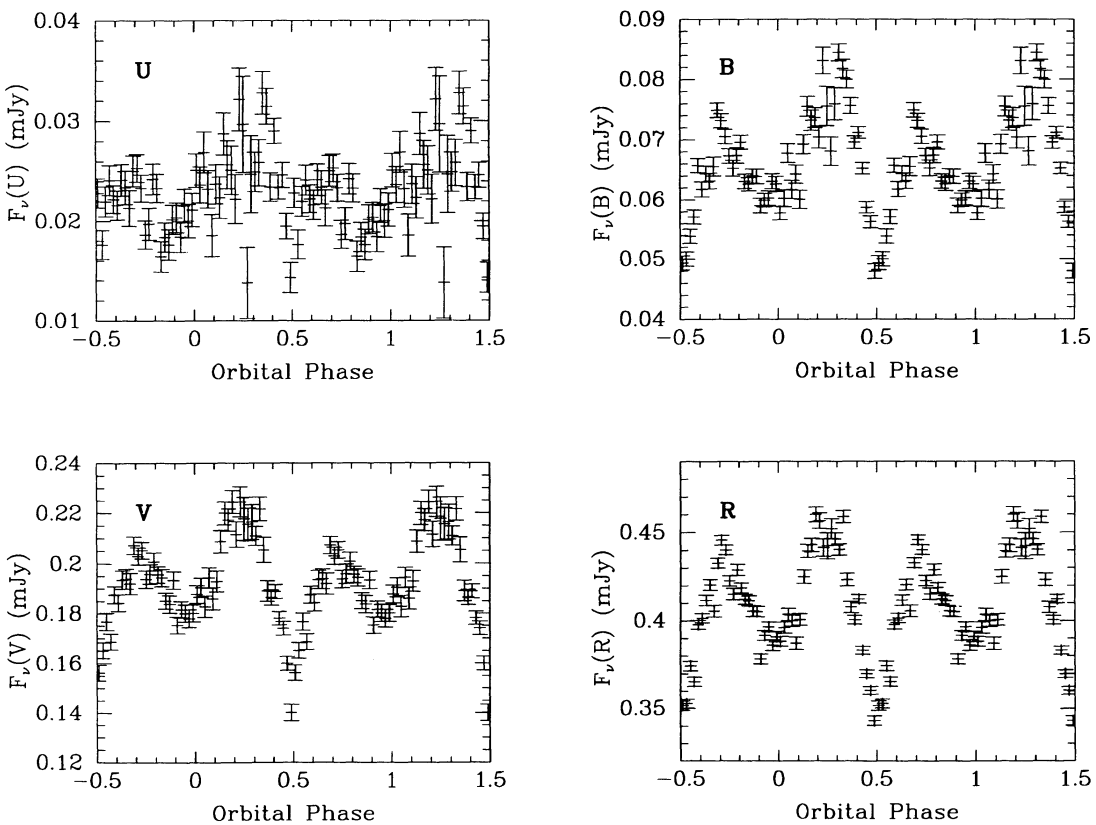

FIG. 1.—The weighted mean multicolor light curves obtained 1986 December/1987 January. This figure (and all subsequent figures) uses the standard orbital phase convention, which is 180° out of phase with the convention used in McClintock & Remillard's (1986) ephemeris. A weighted rebinning to 50 orbital phase bins has been performed, and the data have been plotted twice in order to make the orbital variations more clear. (*a*) The U-band light curve; (*b*) the B-band light curve; (*c*) the V-band light curve; (*d*) the R-band light curve.

of McClintock & Remillard, but in their data (which were taken in 1981–1985) the maximum following phase 0.5 (on the standard convention used herein, this is phase 0.0 according to their ephemeris) is the higher of the two.

In the *B*, *V*, and *R* light curves, the minimum at phase 0.5, which occurs when the secondary star is behind the compact object, is much deeper and sharper than the minimum at phase 0.0. The most plausible explanation for this feature is a grazing eclipse of the Roche lobe-filling star by the accretion disk. The minimum at phase 0.5 (which is phase 0.0 on the McClintock & Remillard ephemeris) was also the deeper in the data published by McClintock & Remillard (1986) but it does not appear to be either as deep or as sharp in their data as it does in our light curves, which have higher phase resolution. In Paper II subsequent observations of A0620−00, in which the eclipse-like feature is not present, will be discussed. This raises the question of whether or not the feature is real, or simply an artifact due, for example, to clouds or dome occulation in one night's data; or to jumps caused by merging partial orbital coverage from nights on which the source had differing average luminosity. To check for these possibilities, the data from the individual nights were compared against each other. In the *B* and the *R* band, data from both 1986 December 30 and 31 unambiguously show the asymmetry between the two minima. The asymmetry is present but less obvious in the December 31 *V* band data, and in the 1987 January 2 data in all colors. This strengthens confidence in the credibility of the eclipse-like feature in the mean light curves. It is highly unlikely that a spurious artifact would arise at phase 0.5 on more than one night. Though no other published light curves show the eclipse of the mass donor by the outer edge of the accretion disk, it has apparently been independently observed: Karitskaya & Bochkarev (1988) discuss a model for A0620−00 in which such an eclipse is present, although the data on which the model is based are not shown.

Figure 2 shows the orbital modulations in color. This figure shows that the light curve is relatively blue before phase 0.5, i.e., the higher of the two maxima in the light curves is bluer than the remainder of the curves. The eclipse at phase 0.5 is clearly relatively red: it appears as a sharp peak in $F_\nu(R)/F_\nu(V)$, and a sharp dip in $F_\nu(B)/F_\nu(V)$. These properties provide important constraints for the modeling of the light curves.

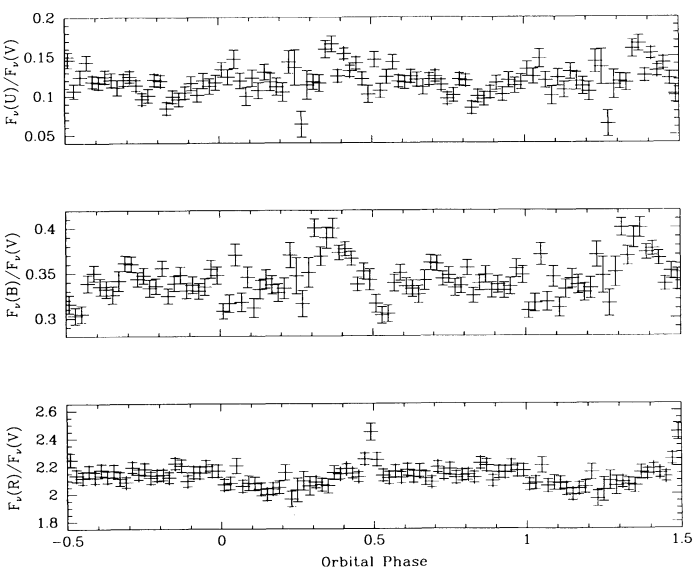

FIG. 2.—The color ratio light curves formed by dividing the *V* band into the simultaneous *U*, *B*, and *R* data. Points from phase 0.0 to 0.5 have been plotted twice. The two lower panels show that the eclipse at phase 0.5 is relatively red, while the maximum at phase 0.25 is relatively blue.

3. LIGHT CURVE MODELING

The orbital light curves were modeled using a code for generating synthetic light curves based on the work of Zhang (1986). The model includes realistic treatments of the geometry, the heating effects, gravity darkening, and limb darkening. A number of modifications to the code, described in Haswell (1992), were implemented. Most of these modifications were made to provide a more realistic treatment of the mass donor star. The most important modification was the introduction of realistic stellar spectra, instead of blackbody spectra, for the grid points on the mass donor. The stellar spectra were taken from the "BKLATE" synthetic spectral atlas of Buser & Kurucz (1988; Buser 1991). The models employ an extensive list of opacity sources and are able to reproduce the observed line-blanketing in the UV with considerable success. Linear limb-darkening coefficients for each of the passbands of the Stiening photometer were interpolated from the $T_{\rm eff}$ = 5000 K, $\log(g) = 4.5$ (cgs units) results of Wade & Rucinski (1985).

The assumption that the mass donor exactly fills the Roche lobe was adopted; the effects of relaxing this assumption are described later. With the Roche lobe-filling constraint applied, the only three parameters that affect the contribution of the mass-losing star to the orbital light curve are (i) the mass ratio, q; (ii) the temperature of the mass donor star at its poles, T_2 (which is also the peak temperature on the star in the absence of strong heating); and (iii) the orbital inclination, i. Heating due to irradiation is an insignificant effect in A0620−00, so the mean effective temperature, $T_{\rm eff}$, is governed by T_2 and the gravity darkening phenomenon. The gravity darkening for each grid point on the Roche lobe-filling star was computed from the relationship $T_{\rm eff} \propto g^\beta$, and the mean effective temperature for the star as a whole is $\sim$100–200 K below the peak temperature. The effective temperature of the mass donor can be directly inferred from the spectral type, though as § 3.1 will show, the deduced orbital inclination is insensitive to this parameter. The analysis to be presented in Paper II favors a spectral type of K3–K4. The maximum plausible value of T_2, the peak secondary star temperature, is $\sim$5400 K, while the minimum plausible value is $\sim$4000 K. Three values of q were used in the light curve modeling work: q = 10.6, as indicated by Haswell & Shafter (1990); a higher value of q = 15.0; and a lower value, q = 5.0.

Previous analyses of ellipsoidal variations either have assumed that the secondary star is the sole source of optical radiation (e.g., Bochkarev, Karitskaya, & Shakura 1979), or have made use of additional information and assumptions to constrain the contribution of the ellipsoidally variable component (e.g., Kuiper, van Paradijs, & van der Klis 1988.) In contrast, our modeling shows that the contribution of the accretion flow to the orbital light curves of A0620−00 is non-negligible.

The contribution from the disk is modeled in two parts. The first part is from the bulk of the disk and produces a contribution which (in the absence of eclipses) is constant with orbital phase. Quantitative analysis which will be presented in Paper II indicates that the higher of the two maxima is too blue to be purely due to the ellipsoidal variation from the K dwarf; there is a contribution at this phase from relatively blue excess emis-

sion from the accretion flow. A precessing elliptical disk model, as invoked for the SU UMa superhump phenomenon, can explain the existence and variability of the excess emission. Thus, the second part of the accretion disk contribution to the light curve is phase-dependent, and is responsible for the boosting of the higher of the two maxima. Alternatively, this component could be viewed as that part of the disk emission that varies with orbital phase, without invoking a detailed model to account for the variations. The nonvarying disk component is modeled as a geometrically thin, circular, isothermal, blackbody disk, surrounding the compact object. This contribution to the light curve depends on (i) the inner radius of the disk, $r_{\rm inner}$; (ii) the outer radius of the disk, $r_{\rm outer}$; (iii) the temperature of the disk, $T_{\rm disk}$; (iv) the limb-darkening coefficient; and (v) the orbital inclination i. The phase-varying disk component depends on: (i) an azimuthal angle which governs the phase at which the flux is maximized; (ii) a temperature, $T_{\rm spot}$; and (iii) a radius, $r_{\rm spot}$, which controls the surface area of the enhanced emitting region.

The fraction of the surface of the mass donor occulted by the accretion disk varies with the orbital inclination, i; the size of the mass donor star, which depends on the mass ratio, q; and the outer radius of the disk, $r_{\rm outer}$. The depth of the eclipse is dependent on the relative contributions of the mass donor and the accretion flow to the total flux. This combination of geometrical factors and constraints on the relative luminosities provides a powerful means of constraining the orbital inclination, i. In fact, without the eclipse a definite constraint on the orbital inclination would have been difficult or impossible. The amplitude of the ellipsoidal variations in the various filters provides one constraint between the flux from the mass donor star, the flux from the accretion flow, and i. The eclipse provides an additional constraint and allows acceptable fits only for a small range of orbital inclinations.

There are thus three features in the observed B, V, and R band orbital light curves that must be adequately reproduced by the synthetic light curves. The first of these is the ellipsoidal variation, which dominates the overall shape of the light curves, and is best isolated in the amplitude between the lower maxima (phase 0.75) and the shallower minima (phase 0.0). This is because the higher maxima are boosted by the phase variable component from the disk, and the deeper minima are affected by a grazing eclipse of the mass donor star. (The shallower minima are affected by the eclipse of the disk by the mass donor, but this eclipse is much less important; a point which is further elaborated below.) The second feature is the asymmetry between the two maxima. The third feature is the eclipse. The U band light curve is noiser than the B, V, and R curves, and does not show these three features clearly. The U band curve apparently contains a contribution from a component not included in the simple model applied here. This component is likely optically thin emission from the disk chromosphere, which is presumably also the source of the observed Balmer emission lines.

As a preliminary to the exploration of parameter space, the azimuthal angle for the phase-varying disk component was determined by matching it to the observed light curves. Once a satisfactory fit for this parameter was found, it was fixed for the remainder of the work. As expected, variations in other parameters did not noticeably affect the phasing of the asymmetry. The adopted angle was 97°, measured at the primary star, with 0° along the line of centers of the two stars, and angle increasing in the direction counter to the orbital motion of the binary system. Other parameters which could in principle be varied, but which were fixed are as follows.

1. The albedo of the mass donor star, which was set to 0.5. This choice is justified by the theoretical calculations of Milgrom & Salpeter (1975) and London, McCray, & Auer (1981), who obtain a variety of values for the albedo, all of which are near 0.5. Heating of the mass donor is not a large effect in A0620−00 in quiescence, so the choice of albedo is not critical.

2. The gravity darkening coefficient, β, was fixed at 0.08, following Sarna (1989). Actually Sarna's paper states $\beta \approx 0.05$ for $M_2 \leq 0.7\ M_\odot$ and $\beta \approx 0.08$ for $M_2 \geq 0.7\ M_\odot$. Many of the model fits to be described below imply $M_2 \leq 0.7\ M_\odot$. Since Sarna's results are based on zero-age main-sequence stellar envelopes, the discriminating parameter between the two choices of β is ultimately the effective temperature. Hence, adopting the higher mass value, appropriate to the effective temperature of the late-type star as revealed by its spectral type, is justified.

3. The limb-darkening coefficients for the mass donor star and disk, which were interpolated from the $T_{\rm eff} = 5000$ K, log $(g) = 4.5$ (cgs units) results of Wade & Rucinski (1985). The values used were: $u(U) = 0.95$; $u(B) = 0.80$; $u(V) = 0.67$; $u(R) = 0.57$.

4. The inner radius of the accretion disk, $r_{\rm inner}$, was set to $0.001a$. This choice is somewhat arbitrary, but the inner radius is not a critical parameter. Since the model disk is assumed to be isothermal, the luminosity is proportional to the surface area: thus the outer disk radius is a much more critical parameter.

In most cases, it was not possible to fit the light curves well in all colors. When this occurred the disk temperature was adjusted, and the iterative adjustment of $T_{\rm spot}$, $r_{\rm spot}$, and i was repeated. Once the full range of possible disk temperatures had been considered, the disk radius, $r_{\rm outer}$, was adjusted, and new solutions sought. When the possibilities for $r_{\rm outer}$ were exhausted, a new choice of T_2 was considered. Finally, the mass ratio, q, was changed, and the entire procedure repeated.

The assumption that the disk is geometrically thin and circular minimizes both the luminosity of the disk and the depth of the eclipse for a given (i, $r_{\rm outer}$) pair. If the possibility of a vertically extended disk were admitted, then the surface area of the disk, and the fraction of the late-type star occulted by it would increase. If the disk in A0620−00 is vertically extended, then the model fits will give a larger value of $r_{\rm outer}$ than is actually the case.

The model does not address the effect of a noncircular disk on the relationship between the emitting surface area and the fraction of the secondary star which is occulted in an eclipse. If the largest radius part of the disk is aligned along the line of centers of the two stars, then a fit to the eclipse will overestimate the mean disk radius. If the smallest disk radius is aligned with the line of centers, an eclipse fit will similarly underestimate the mean disk radius. Lacking the quality of data necessary to discern between the possibilities, the circular disk model must suffice. The disk is expected to be truncated by tidal forces at the tidal radius. However, the effects of a vertically extensive disk would be similar to those of an increased disk radius. The simulations of Whitehurst (1988) show that in some cases the disk extends out to the critical Roche equipotential surface so the possibility of the disk radius exceeding the tidal radius was considered in the modeling: radii up to that of

the largest circular disk which would fit inside the primary Roche lobe were considered.

The goodness of fit of the synthetic light curves was quantitatively determined by comparing the mean values of the observed and calculated light curves in four phase bins centered on phases 0.0, 0.25, 0.5, and 0.75. These four phases correspond to the two maxima and minima in the light curve, and the calculated light curve must correctly reproduce the asymmetry in the maxima, the ellipsoidal amplitude, and the eclipse depth if the curves are to agree at all four phases. Since the formal errors associated with the observed light curves do not include systematic errors in the data reduction, they underestimate the true errors. The synthetic light curves are derived from a very simple model, and consequently may not fully reproduce the actual shape of the observed curves. Thus, synthetic light curves which agreed with the observed values to within 3 standard deviations (calculated from the formal errors in the observed data) were deemed to be acceptable fits. χ^2 for the entire light curve was also calculated for each of the fits. The formal errors underestimate the true uncertainties (because they do not include errors in the sky subtraction; the deviations from the true orbital light curve caused by flickering on time scales longer than 100 s; or by night-to-night variations) so χ^2 is larger than statistically predicted for an acceptable model. Figure 1 shows that the point-to-point deviations in the light curves are typically larger than the formal error, therefore the smooth model fits will necessarily have larger values of χ^2 than formally predicted for a model which fits the data. χ^2 increases by about 1% for a 1° change in the orbital inclination from the best fitting model for a given (q, T_2, $T_{\rm disk}$) parameter set. Examining the deviations in the four phase bins used to determine the acceptability of the fit is a much more sensitive indicator of the orbital inclination, as the grazing eclipse of the mass donor by the disk changes rapidly with small adjustments to the orbital inclination, while the remainder of the light curve remains almost unchanged. The values of χ^2 for each color and the total χ^2 are tabulated for each of the acceptable fits in Tables 1–3. The total χ^2 is roughly the same for all the acceptable models, and in all cases is dominated by the contribution from the R-band light curve. This is because the formal errors in the R band are particularly small compared to the point-to-point deviations, an artifact likely due to flaring in the source. The signal-to-noise ratio of the data presented here does not permit individual flares to be identified with ease, but data to be presented in Paper II show clear evidence for flares.

The synthetic light curves were each normalized independently so that the mean values of the observed and calculated curves agreed for each passband. This means that the absolute color information in the photometry is not used to constrain the fit. Hence the deduced parameters are not affected by the value adopted for the reddening. The results of the light curve modeling were previously reported in Haswell (1992); minor numerical errors in those results were discovered, so the values reported here differ slightly. The final code was checked against independently developed software, and the output from the corrected code was rechecked analytically.

3.1. *Results:* q = 10.6

The first secondary star temperature to be considered was $T_2 = 4600$ K; this choice of T_2 corresponds to a K4 spectral type. A summary of the parameters of models producing successful fits to the orbital light curves is given in Table 1. As the table shows, for the first three models, the disk radius, $r_{\rm outer}$, was set to 0.60a. This is the radius of the maximum circular disk fitting inside the primary Roche lobe for a system with a mass ratio of 10.6. The comparison of the synthetic and observed light curves for the model designated "F2" in Table 1 are given in Figure 3, and the component contributions to these synthetic light curves are shown in Figure 4.

Figure 3 shows that the model fit is good for the B, V, and R light curves. The fit for the U-band light curve is not so good: the amplitude of the variations seems to be higher in the synthetic light curve than in the observed curve, indicating the presence of an additional unmodeled source of flux in the observed light curve. If Wu et al.'s (1976) reddening is used to deredden the observed light curves, the synthetic light U-band light curve is too faint, supporting this conclusion. Some

TABLE 1

SUMMARY OF SUCCESSFUL FITS FOR $q = 10.6$

Label	Secondary Star Temperature T_2 (K)	Disk Temperature $T_{\rm disk}$ (K)	Disk Radius $r_{\rm outer}$ (a)	Orbital Inclination i	χ^2_U	χ^2_B	χ^2_V	χ^2_R	$\chi^2_{\rm total}$
F1	4600	4200	0.60[a]	67°.5	240	333	181	495	1250
F2	4600	4000	0.60[a]	66	260	320	176	484	1240
F3	4600	3800	0.60[a]	65	326	340	185	524	1375
F4	4600	4000	0.55[b]	68	281	333	185	544	1342
F5	4600	4200	0.55[b]	69	255	322	178	489	1245
F6	4600	4200	0.53	70	257	331	181	539	1308
F7	5000	4400	0.60[a]	66.5	252	325	177	483	1237
F8	5000	4200	0.60[a]	65.5	277	326	173	498	1274
F9	5000	4000	0.60[a]	64.5	298	344	183	542	1369
F10	5000	4600	0.55[a]	69.5	232	345	175	475	1228
F11	5000	4400	0.55[b]	68.5	253	342	176	504	1275
F12	5000	4200	0.55[b]	67.5	270	358	180	517	1324
F13	5000	4600	0.53	70	242	337	176	514	1271
F14	5000	4400	0.53	69	262	343	179	518	1301
F15	5000	4600	0.51	70.5	253	339	183	539	1313

[a] This radius is the maximum radius for a circular disk inside the compact object Roche lobe.
[b] This radius is the tidal radius following Pacyński 1977.

TABLE 2

SUMMARY OF SUCCESSFUL FITS FOR $q = 15$

Label	Secondary Star Temperature T_2 (K)	Disk Temperature T_{disk} (K)	Disk Radius r_{outer} (a)	Orbital Inclination i	χ^2_U	χ^2_B	χ^2_V	χ^2_R	χ^2_{total}
G1	4600	3800	0.63[a]	66°.5	268	343	173	464	1248
G2	4600	4200	0.57[b]	71	241	332	179	474	1225
G3	4600	4000	0.57[b]	70	282	340	181	502	1306
G4	4600	4400	0.53	73.5	245	336	181	510	1272
G5	5000	4200	0.63[a]	67.25	280	341	174	476	1271
G6	5000	4000	0.63[a]	65.75	297	345	178	495	1315
G7	5000	4600	0.57[b]	71.5	250	335	178	484	1246
G8	5000	4400	0.57[b]	70.5	278	342	178	492	1290
G9	5000	4800	0.54	73.25	243	336	181	496	1256
G10	5000	4600	0.54	72.25	263	338	179	491	1284
G11	5000	4800	0.52	73.5	233	350	180	491	1254

[a] This radius is the maximum radius for a circular disk inside the Roche lobe of the compact object.
[b] This radius is the tidal radius following Pacyński 1977

models were run with a 8000 K hot inner disk component. They were successful in improving the fit to the U-band light curve, but the models failed in a more important capacity: the relative depths of the B, V, and R-band eclipses could no longer be reproduced. The B-band synthetic eclipse was too shallow, while that of the R band was too deep. It seems that the U band contains a contribution from a component which is not well reproduced by the simple model adopted here. Optically thin chromospheric emission could provide the additional U-band flux, without producing the additional B-band flux that causes difficulties in fitting the relative depths of the eclipses. To preserve the simplicity of the model, the goal of simultaneously fitting the U-band light curve was abandoned. The tightest constraints on the orbital inclination arise from the eclipse at phase 0.5, which is not readily apparent in the U-band light curve. Hence, we are not discarding information directly relevant to the issue of the component masses. With a more sophisticated model we may, however, have learned more about the accretion disk.

Figure 4 shows that just over half of the flux arises in the bulk of the accretion disk, with most of the remainder coming from the mass donor. The mass donor contribution exhibits ellipsoidal variations and the grazing eclipse at phase 0.5. The corresponding eclipse of the disk at phase 0.0 is very much shallower for three reasons. First the deepest minimum in the mass donor contribution occurs at phase 0.0 even in the absence of an eclipse, because the region of the mass donor around the L1 point is gravity-darkened. Second, the fraction of the visible mass donor surface area which is occulted is much higher than the occulted fraction of the disk, because the disk has a larger projected surface area. Third, the surface flux from the disk is lower due to the lower effective temperature used to model it and is heavily limb-darkened because of the high orbital inclination. The eclipsed surface of the mass donor is much more closely aligned to the plane of the sky; hence limb darkening is much less severe. In models in which the difference between T_2 and T_{disk} is greater, the proportion of the flux from the mass donor is higher.

TABLE 3

SUMMARY OF SUCCESSFUL FITS FOR $q = 5$

Label	Secondary Star Temperature T_2 (K)	Disk Temperture T_{disk} (K)	Disk Radius r_{outer} (a)	Orbital Inclination i	χ^2_U	χ^2_B	χ^2_V	χ^2_R	χ^2_{total}
H1	4600	4200	0.53[a]	63°.5	282	313	180	537	1269
H2	4600	4000	0.53[a]	63	288	315	182	590	1376
H3	4600	4400	0.50[b]	66	227	320	178	527	1252
H4	4600	4200	0.50[b]	65	260	315	182	572	1329
H5	4600	4000	0.50[b]	64	296	325	175	529	1325
H6	4600	4400	0.47	67	257	315	181	590	1343
H7	4600	4200	0.47	66	260	328	174	523	1286
H8	4600	4400	0.45	67.5	262	321	179	564	1327
H9	5000	4600	0.53[a]	64	229	317	175	536	1257
H10	5000	4400	0.53[a]	63	257	310	181	573	1321
H11	5000	4200	0.53[a]	62.5	293	324	181	592	1389
H12	5000	4600	0.50[b]	65	246	316	183	564	1308
H13	5000	4400	0.50[b]	64.5	280	320	177	576	1353
H14	5000	4800	0.47	67	250	314	180	589	1334
H15	5000	4600	0.47	66	260	324	175	420	1279
H16	5000	4800	0.45	67.5	257	321	179	558	1314

[a] This radius is the maximum radius for a circular disk inside the Roche lobe of the compact object.
[b] This radius is the tidal radius following Pacyński 1977.

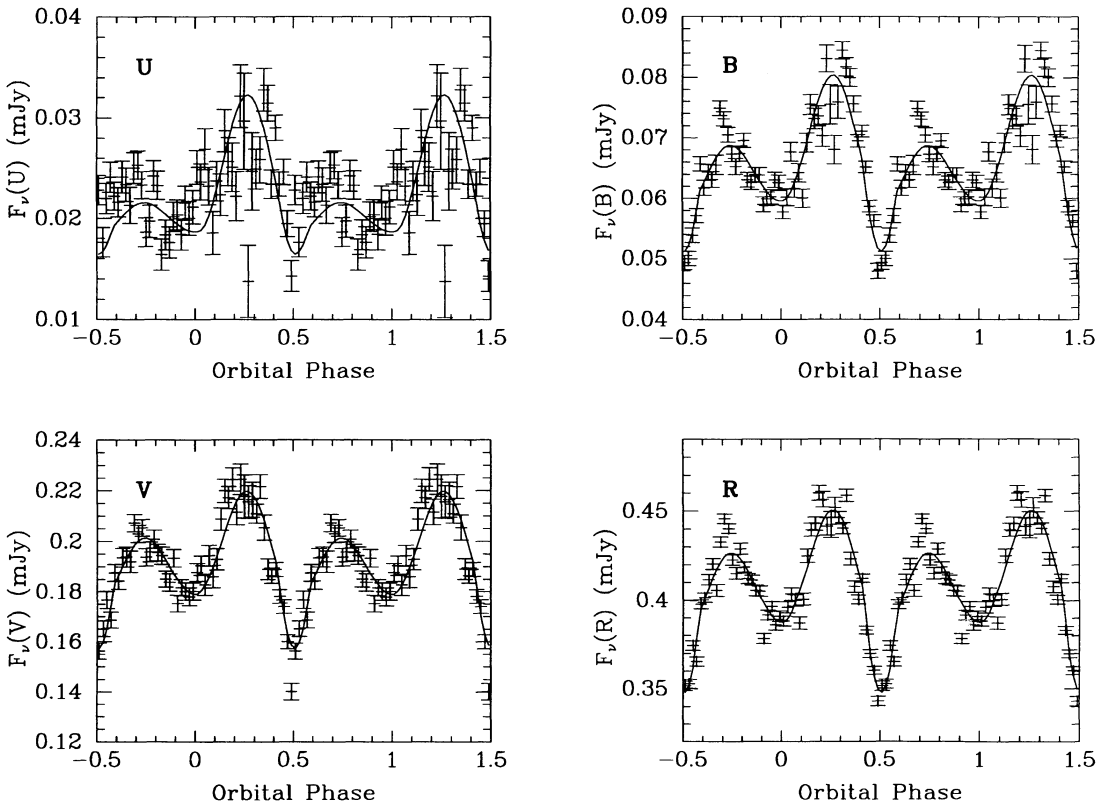

FIG. 3.—The U, B, V, and R band synthetic light curves from model F2 (described in Table 1) superposed on the observed light curves. The U-band curve fit is not very good; the amplitude of the variations in the synthetic curve is higher than in the observed light curve. In the B, V, and R bands the fits are much better: the synthetic curves reproduce the mean heights of the two maxima, and the depths of the minima at phase 0.0; the depths of the eclipses at phase 0.5 are fit tolerably. This model uses a disk temperature at the upper end of the range that produces acceptable fits. The light curve is relatively red during the eclipse, and the relative depths of the eclipses are better reproduced by models in which the temperature difference between the disk and the mass donor star is greater. In this fit the B and V-band synthetic eclipses are not as deep as in the observed light curves, though they are within the deviation permitted for the fit to be deemed acceptable.

Table 1 shows the results of a systematic search in parameter space for models that fit the B, V, and R light curves. For each (q, T_2, r_{outer}) combination, fits are found for a range of disk temperatures. At the upper end of the range, the color of the disk is too blue to allow the relative amplitudes of the ellipsoidal variations, or the color at the eclipse to be reproduced. At the lower end of the range, the disk flux is too low to dilute the ellipsoidal variations sufficiently. A range of orbital inclinations is thus found for each (q, T_2, r_{outer}) combination, the highest inclinations arising from the hottest choice of disk temperature. When r_{outer} is decreased, the range of satisfactory disk temperatures decreases: the temperature at which insufficient disk flux is generated increases because the emitting surface area has been decreased. The grazing eclipse by the smaller disk occurs at higher orbital inclination, so the deduced orbital inclinations are higher. Eventually, r_{outer} becomes small enough that no fits are found: to be bright enough to dilute the ellipsoidal variations, the disk is required to be too blue to fit the eclipse colors. Thus, though there is no a priori lower limit on the disk radius, for a given value of T_2 the modeling provides a strict constraint. Once the mass ratio, q, and the secondary star temperature, T_2, are specified there is a very small area of parameter space which produces satisfactory fits. A similar conclusion regarding the disk radius was reached by Karitskaya & Bochkarev (1988). They state that the disk radius is variable and the disk often nearly fills the Roche lobe of the primary star. Both these findings are supported by the results reported herein and in Paper II.

Table 1 shows results for two choices of T_2; the results are similar in both cases: the orbital inclination depends upon the value of $T_2 - T_{disk}$, rather than upon T_2 itself. Hence the deductions about the orbital inclination and consequently M_1 are essentially independent of the spectral type adopted for the mass donor.

Some models were run using a secondary star underfilling its Roche lobe by more than 15% in volume. Compared with the corresponding results for a Roche lobe-filling secondary, the orbital inclination increased by 4°. Such severe underfilling of the Roche lobe is extremely unlikely, because mass transfer would not be expected to occur at all in this case.

3.2. *Results* q = 15.0

The systematic search of parameter space was repeated for $q = 15.0$. With this mass ratio the secondary star radius is a smaller fraction of the orbital separation of the two stars, so the light curve fits are expected to exhibit larger orbital inclinations than those for $q = 10.6$. This is indeed the case, as shown in Table 2. The same factors as discussed above limit the successful fits to a small region in parameter space.

3.3. *Results* q = 5.0

With this mass ratio the secondary star radius is a larger fraction of the orbital separation, and consequently the deduced orbital inclinations are lower than for the mass ratios previously considered. The results of the search in parameter space for $q = 5.0$ are given in Table 3.

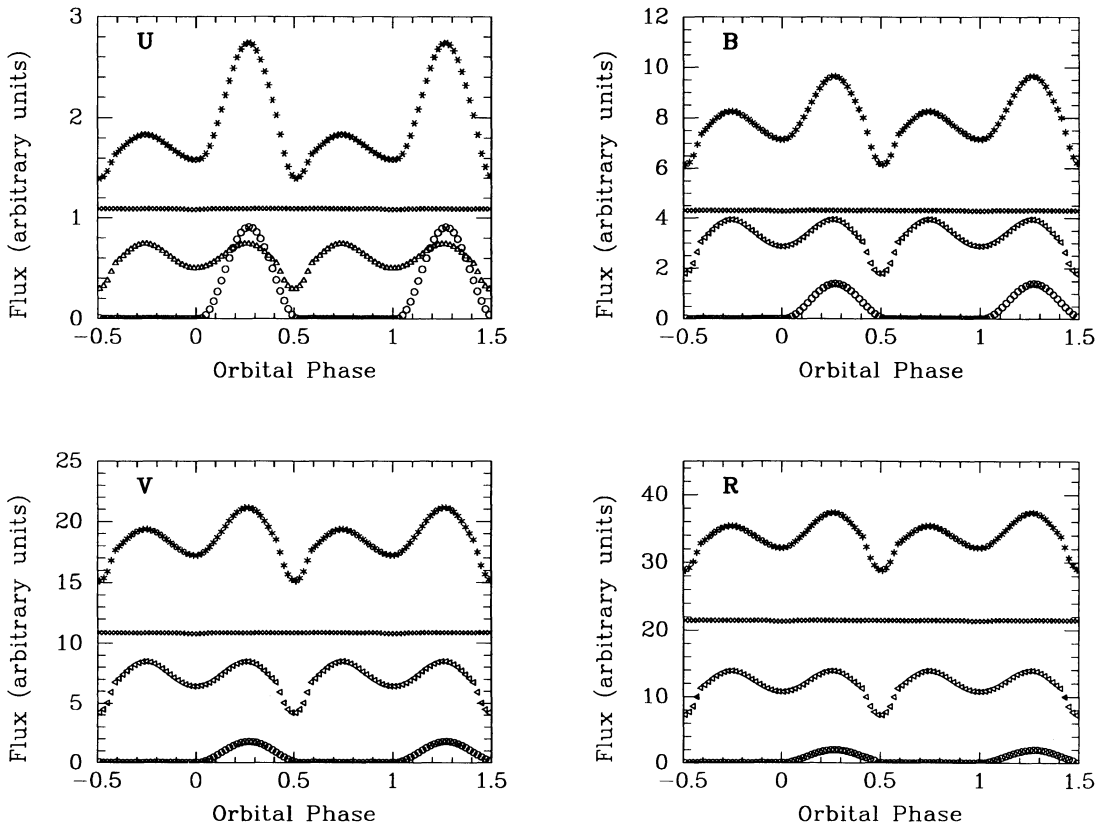

FIG. 4.—The component contributions to the synthetic light curves shown in Fig. 3. The contribution from the bulk of the accretion disk is plotted in crosses and remains constant except for the very shallow eclipse at phase 0.0; the phase-varying disk component is plotted in open circles and is responsible for boosting the higher of the two maxima. The contribution from the Roche lobe-filling star is plotted in triangles. This component shows ellipsoidal variations, along with the grazing eclipse of the mass donor by the disk. This eclipse appears much deeper than the eclipse of the disk by the mass donor. The total flux is plotted in asterisks.

3.4. *Summary*

Acceptable fits to the orbital light curves were found for all three mass ratios considered. The orbital inclinations obtained were insensitive to the choice of T_2, but were dependent on the difference between the temperatures of the mass donor and disk. For $q = 10.6$, the range of orbital inclinations for which acceptable or marginally acceptable fits are obtained is $64\overset{\circ}{.}5 \leq i \leq 70\overset{\circ}{.}5$. With a mass ratio $q = 15.0$, $65\overset{\circ}{.}75 \leq i \leq 73\overset{\circ}{.}5$ was found. The lowest mass ratio considered, $q = 5.0$, leads to orbital inclinations in the range $62\overset{\circ}{.}5 \leq i \leq 67\overset{\circ}{.}5$. The values determined are somewhat dependent on the model adopted for the disk: the introduction of a hot inner disk component increases the best fitting orbital inclination by $\sim 1°$ (while degrading the quality of the eclipse fits). However, the constraints enforced by the eclipse depths and the ellipsoidal amplitudes are strong, so that even with a significantly different temperature distribution for the disk, neither limit on the orbital inclination is likely to change by more than a few degrees for given values of q and T_2.

An implausibly severe underfilling of the mass donor Roche lobe (an underfilling by more than 15% by volume) leads to an increase in the orbital inclination of 4°. Thus the assumption that the mass donor is Roche lobe-filling does not critically affect the deduced limits on the orbital inclination.

The combination of the spectral type, the eclipse depths, and the fractional amplitude of the ellipsoidal variations produce strong constraints on the size of the accretion disk. As Figure 2 shows, the spectrum is redder in eclipse than out of eclipse; this means that the flux from the accretion disk must be redder than the flux from the K star. A blackbody disk cool enough to reproduce the color of the eclipse must be large to dilute the flux from the Roche lobe-filling star sufficiently to reproduce the observed fractional amplitudes of the ellipsoidal variations. All the successful fits required accretion disk outer radii comparable to the Paczyński tidal radius. A similar conclusion was reported by Karitskaya & Bochkarev (1988).

Note that if the quiescent disk emission is optically thin, then the red color temperature is more likely due to the Paschen continuum emission rather than to low-temperature blackbody emission. In this case the actual temperature would be higher than that indicated by the color of the disk, and the surface flux from the disk could exceed that of the blackbody used to model it. Consequently the constraint on the area and hence the orbital inclination would be weakened. The effects of relaxing this assumption were examined quantitatively by allowing the temperature $T_{\rm disk}$ to vary from filter to filter for otherwise simultaneous fits. This is equivalent to fitting a disk brightness temperature to each filter, without assuming the disk emits as a blackbody. Using a higher brightness temperature, the surface flux increases, and the disk area can decrease while still diluting the ellipsoidal variations to the same extent. With a reduced disk radius, the inclination required to reproduce the grazing eclipse at phase 0.5 is increased. However, the shape of the light curves precludes an

increase in inclination of more than a few degrees. This is because the grazing eclipse of the disk by the mass donor is shallow. By increasing the surface flux and the inclination a deeper eclipse at phase 0.0 is produced. Increasing the inclination also has the effect of increasing the ellipsoidal variation, and simultaneously decreasing the observed disk flux which dilutes it. In Figure 5 this is illustrated. The first three panels show the R-band fits for models F7, F10, and F15. The last panel shows a model generated with the parameters of model F15, but with a disk of half the area and twice the surface brightness of model F15. In order to reproduce the phase 0.5 eclipse, the inclination was increased from 70°.5, as used in model F15, to 75°. The increase in inclination results in eclipse at phase 0.0 which is clearly much deeper than observed. In addition, the ellipsoidal maxima are slightly too high. Therefore, even if the blackbody assumption is relaxed, for a uniform disk, the limits on the orbital inclination cannot increase by as much as 4°.5. If, however, the inner disk was much brighter than the outer parts, then it would be possible to reproduce the deep eclipse at phase 0.5 without introducing a substantial eclipse at phase 0.0.

4. MASS DETERMINATION

Haswell & Shafter (1990) measured the radial velocity variations of the Hα emission line. If the variation is interpreted as directly reflecting the orbital radial velocity of the compact object, then $K_1 = 43 \pm 8$ km s^{-1} and $q = K_2/K_1 = 10.6 \pm 2.0$ (using the McClintock & Remillard 1986 measurement of K_1). There are indications, however, that the radial velocity variations are not purely due to orbital motion. The most obvious of these indications is the 60° discrepancy between the phase of the observed emission-line velocity curve and that implied for the primary star by the well-defined absorption line velocity curve of the mass donor. An attractive explanation for the secular variations in the orbital light curve is a model involving a precessing elliptical disk; this will be discussed in Paper II. The non-Keplerian disk motions implied by this model potentially invalidate any deduction of the compact object orbital motion from the radial velocity shifts of the disk lines, since the method requires that the emission from the disk itself be axisymmetric. (The effects of additional nonaxisymmetric contributions from the mass donor or the bright spot were considered in detail by Haswell & Shafter 1990.) In spite of this, the case for the detection of the primary orbital motion is not hopeless: the evidence for a precessing elliptical disk was no longer apparent in the orbital light curve by the end of 1989, when the spectroscopic data used by Haswell & Shafter (1990) were taken. So Haswell & Shafter's (1990) value of K_1 should be considered a plausible best estimate.

Supporting evidence for $q \sim 10$ is provided by a completely independent observation. Assuming that the secondary star is in corotation with the orbital motion, the rotational broaden-

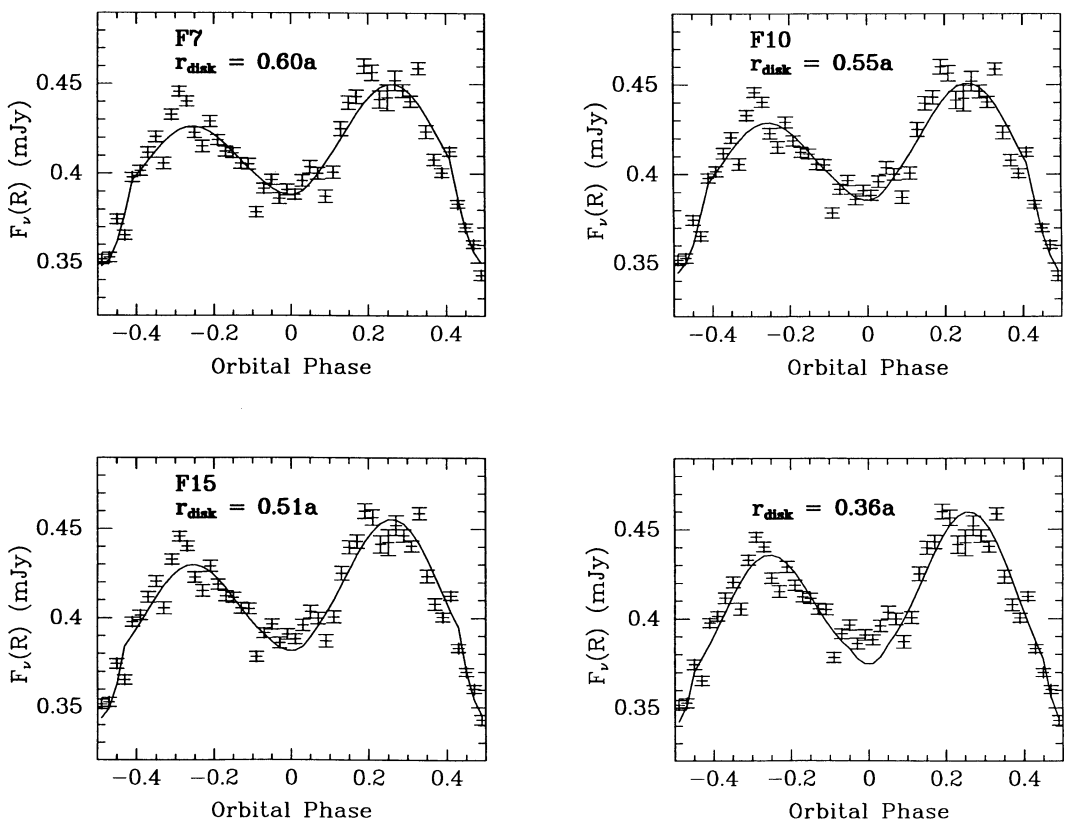

FIG. 5.—R-band models illustrating the lower limit on the disk radius, even if the blackbody assumption for the disk is relaxed. The first three panels show the R-band fits for models F7, F10, and F15. Model F15 leads to the upper limit on the inclination, and lower limit on the disk radius in the case of a blackbody disk. The minimum at phase 0.0 in model F15 is deeper than in the observed light curve but is close enough to be acceptable. If the blackbody assumption is relaxed, a model analogous to F15 can be generated with a disk of half the area and twice the surface brightness. Such a model is shown in the fourth panel. In order to reproduce the eclipse depth at phase 0.5, an inclination of 75° was required. This leads to an eclipse of the disk by the mass donor at phase 0.0 which is clearly too deep to fit the observations. Thus, even if the blackbody assumption is abandoned, the orbital inclination cannot increase by as much as 4°.5.

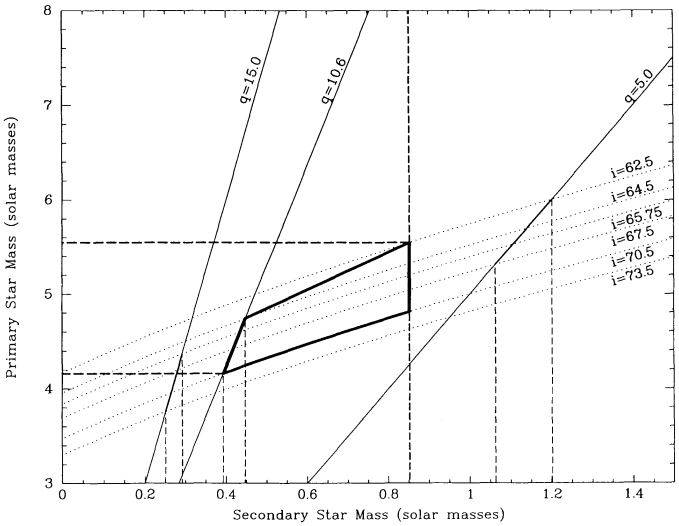

FIG. 6.—Component masses for A0620−00: solid lines show loci of constant mass ratio; dotted lines represent loci of constant orbital inclination. Constraints on i for $q = 5.0$, $q = 10.6$, and $q = 15.0$ are delineated with a bold line segment for each of the three mass ratios. The vertical dashed lines dropped from the constant q loci outline the implied values of M_2 for each of the three mass ratios. The bolder vertical dashed line corresponds to the upper limit on M_2 corresponding to a Roche lobe-filling main-sequence star. The heavy solid quadrilateral outlines the region of parameter space indicated for the component masses in A0620−00. As argued in the text, the mass ratio is unlikely to be more extreme than 10.6, leading to the limit on the left-hand side of the quadrilateral. The right-hand side of the region is bounded by $M_2 \leq 0.85$. This limit constrains the mass ratio to be greater than $q = 5.0$. Thus, adopting the limit $i < 62°.5$, that obtained for $q = 5.0$, gives a safe lower limit on the orbital inclination, represented in the upper bound on the favored region. The upper bound on i: 70°.5, corresponds to the limit obtained for $q = 10.6$. The dashed horizontal lines outline the limiting values for the mass of the compact object.

ing of the absorption lines from the secondary can be used to deduce the mass ratio: a mass ratio of $q \approx 9$ (which implies $K_1 \approx 50$ km s^{-1}) is indicated (McClintock 1992).

The implications of the light curve modeling for the masses of the component stars are shown in Figure 6. The solid lines show loci of constant mass ratio, $q = 15.0$, $q = 10.6$, and $q = 5.0$. Dotted lines represent loci of constant orbital inclination using McClintock's (1992) mass function $f(M_1) = 2.91 \pm 0.08\ M_\odot$. The deduced constraints on i are delineated with a bolder line segment for each of the three mass ratios considered; vertical dashed lines dropped from the constant q loci outline the implied values of M_2 for each of the three values of q. These results are also given in Table 4. The errors quoted in Table 4 reflect the formal errors from McClintock's (1992) mass function. They do not include any systematic errors which may result from the assumptions made in light curve modeling work.

Patterson (1984) gives a prescription for calculating the mass of a Roche lobe-filling, main-sequence secondary from the orbital period, P. It uses an empirically defined ZAMS and a spherical approximation to Roche geometry, and yields $M_2 = 0.85\ M_\odot$ for a period of 7.75 hr. Echevarría (1983) shows that in general the secondary stars in the cataclysmic variable stars have later spectral types than would be expected for main-sequence Roche lobe-filling stars. This is also the case for A0620−00: the mid K spectral type implies a main-sequence mass well below $0.85\ M_\odot$. If the secondary star in A0620−00 were evolved, or if the Roche lobe were underfilled, a mass smaller than the Roche lobe-filling main-sequence star mass would result, so $0.85\ M_\odot$ can be considered an upper limit on the secondary star mass. For $q = 5.0$ the secondary star mass must be higher than $0.85\ M_\odot$ (Fig. 6), so a mass ratio of $q = 5.0$ can be ruled out.

We can derive an estimate of the secondary star mass from its spectral type, though Echevarría's (1983) work suggests that the mass is likely to be higher than this estimate. Gray (1988) gives masses of $\sim 0.75\ M_\odot$ and $0.70\ M_\odot$ for K3 V and K4 V stars, respectively. Taking a lower limit of $i \geq 62°.5$ (obtained for $q = 5.0$) and an upper limit of $i \leq 70°.5$ (obtained for $q = 10.6$), and assuming a main-sequence mass of K3 V–K4 V for the secondary implies $4.6 \leq M_1 \leq 5.4$ and $6.6 \leq q \leq 7.2$. Thus, the spectral type of the mass donor indicates a range of M_2 significantly higher than that obtained from light curve modeling with a mass ratio of 10.6, the case for the $q = 15.0$ is even worse. This implies that the mass ratio is unlikely to be as extreme as 15.0, and mass ratios less than or equal to 10.6 are to be favored.

Since the spectral type of the mass donor is somewhat uncertain, and it is by no means clear that it has a main-sequence mass, the uncertainty in M_2 is much larger than Gray's (1988) mass range. Figure 6 gives a more realistic set of limits. The preferred region for the component masses in A0620−00 is indicated by the bold quadrilateral. The upper limit on M_2 is taken from Patterson's (1981) Roche lobe-filling mass. The limit on the left-hand side of the quadrilateral can be taken from the constraint $q \geq 10.6$. This limit is suggested by the following considerations.

1. It avoids a severely undermassive mass donor;
2. it agrees with the assessment of the systematic errors on K_1 (Haswell & Shafter 1990);
3. it agrees with McClintock's (1992) estimate of q from $V_{\rm rot} \sin i/K_2$;
4. it is favored from an evolutionary standpoint: the formation of a high-mass ratio binary is difficult to explain with existing binary star evolution theory.

The upper and lower bounds on M_1 are derived from the inclination limits implied by the light curve modeling. The upper right-hand corner of the preferred region is given by

TABLE 4

SUMMARY OF RESULTS

	i		M_1		M_2	
q	Lower Limit	Upper Limit	Lower Limit ($M_\odot$)	Upper Limit	Lower Limit ($M_\odot$)	Upper Limit
5.0.....	62°.5	67°.5	5.31 ± 0.15	6.00 ± 0.16	1.06 ± 0.03	1.20 ± 0.03
10.6.....	64.5	70.5	4.16 ± 0.11	4.74 ± 0.13	0.39 ± 0.01	0.45 ± 0.01
15.0.....	65.75	73.5	3.76 ± 0.10	4.37 ± 0.12	0.25 ± 0.01	0.29 ± 0.01

$i \geq 62.^{\circ}5$, obtained from modeling with $q = 5.0$. Since the lower limit on i increases as q increases, and the mass of the secondary star implies that the mass ratio is greater than $q = 5.0$, this is a safe upper limit. The lower limit on M_1 is directly obtained from the upper limit on i for $q = 10.6$.

These limits imply

$$4.16 \pm 0.11 \leq \frac{M_1}{M_\odot} \leq 5.55 \pm 0.15 . \quad (1)$$

The errors given in this inequality reflect only the formal errors resulting from the McClintock (1992) mass function. The systematic data reduction errors are unlikely to exceed the 3 σ limit which was used to determine the allowable region of parameter space in the light curve modeling, so should not significantly affect the result. More importantly, however, there are systematic uncertainties associated with the assumptions used in the light curve modeling. If the simple model we used for the system is incorrect, then it is possible that our deduced orbital inclinations are erroneous. However, even if either the blackbody assumption for the disk is incorrect, or the mass donor substantially underfills its Roche lobe, the upper limits on the orbital inclination do not increase by as much as 5°.

The limits on the mass of the compact object place it substantially above Chitre & Hartle's (1976) upper limit of ~ 3 $M_\odot$ for the mass of a nonrotating neutron star. The limiting mass of 3.76 $M_\odot$ for a maximally rotating neutron star, obtained from Friedman & Ipser's (1987) work, is over 4 σ below the lower limit on M_1 given in inequality (1). Even in the unlikely case of the mass ratio being as extreme as $q = 15.0$, the lower limit on M_1 is at the upper limit on the mass of a maximally rotating neutron star. It would be difficult to reconcile the evidence presented herein with the presence of a neutron star in A0620−00.

Note added in manuscript.—Marsh, Robinson, & Wood (1993) find a mass ratio of $q = 15.9 \pm 2.5$ (using our definition of q) from measurements of the rotational broadening of the absorption lines from the mass donor. This contradicts the preliminary result of $q \approx 9$ reported earlier by McClintock (1992), using the same approach. The new work implies that the upper limit of $q \geq 10.6$ which we adopted in § 4 is incorrect. The light curve modeling results we report for $q = 15.0$ lead to a lower limit of $M_1 \geq 3.76 \pm 0.10$; thus, the possibility of a maximally rotating neutron star is admitted. This model seems unlikely, however, as it would require an equation of state stiffer than any hitherto proposed, as well as the extreme rotation rate. Even for $q = 15.0$ our results show that the compact object mass is well above the commonly accepted 3.2 $M_\odot$ upper limit on the mass of a neutron star.

We are grateful to Dr. Er-Ho Zhang for the use of the light curve modeling codes he developed. Support for this work was provided by NASA grant NAGW-2678. C. A. H. gratefully acknowledges support from Zonta International Amelia Earhart fellowships.

REFERENCES

Bochkarev, N. G., Karitskaya, E. A., & Shakura, N. I. 1979, Soviet Astron. 23, 8
Buser, R. 1991, private communication
Buser, R., & Kurucz, R. L. 1988, in The Impact of Very High S/N Spectroscopy on Stellar Physics, ed. G. Cayrel de Strobel & M. Spite (Dordrecht: Reidel), 531
Chitre, D. M., & Hartle, J. B. 1976, ApJ, 207, 592
Echevarría, J. 1983, Rev. Mexicana Astron. Af., 8, 109
Elvis, M., Page, C. G., Pounds, K. A., Ricketts, M. J., & Turner, M. J. L. 1975, Nature, 257, 656
Friedman, J. L., & Ipser, J. R. 1987, ApJ, 314, 594
Gray, D. F. 1988, Spectral Line Analysis of F, G, and K Dwarfs, Appendix B (Ontario: Aylmer Express Ltd.)
Haswell, C. A. 1992, Ph.D. thesis, Univ. Texas at Austin
Haswell, C. A., Robinson, E. L., Abbott, T. M. C. A., & Horne, K. 1993, ApJ, in preparation (Paper II).
Haswell, C. A., Robinson, E. L., & Horne, K. 1990, in Accretion Powered Compact Binaries, ed. C. W. Mauche (Cambridge: Cambridge Univ. Press), 11
Haswell, C. A., & Shafter, A. W. 1990, ApJ, 359, L47
Horne, K., & Stiening, R. F. 1985, MNRAS, 216, 933
Johnston, H. M., Kulkarni, S. R., & Oke, J. B. 1989, ApJ, 345, 492
Karitskaya, E. A., & Bochkarev, N. G. 1988, Perem. Zvezdy, 22, 943
Kuiper, L., van Paradijs, J., & van der Klis, M. 1988, A&A, 203, 79
London, R., McCray, R., & Auer, L. H. 1981, ApJ, 243, 790
Marsh, T. R., Robinson, E. L., & Wood, J. H. 1993, in preparation
McClintock, J. E. 1992, in Texas/ESO-CERN Symposium on Relativistic Astrophysics, Cosmology, and Fundamental Physics, 1990, Brighton, England, ed. J. D. Barrow, L. Mestel, & P. A. Thomas (New York: NY Acad. Sci.)
McClintock, J. E., & Remillard, R. A. 1986, ApJ, 308, 110
Milgrom, M., & Salpeter, E. E. 1975, ApJ, 196, 583
Oke, J. B. 1977, ApJ, 217, 181
Paczyński, B. 1977, ApJ, 216, 822
Patterson, J. 1984, ApJS, 54, 443
Rhoades, C. E., & Ruffini, R. 1974, Phys. Rev. Lett., 32, 324
Sarna, M. J. 1989, A&A, 224, 98
Wade, R. A., & Rucinski, S. M. 1985, A&AS, 60, 471
Whelan, J. A. J., et al. 1977, MNRAS, 180, 657
Whitehurst, R. 1988, MNRAS, 232, 35
Wu, C.-C., Aalders, W. G., van Duinen, R. J., Kester, D., & Wesselius, P. R. 1976, A&A, 50, 445
Zhang, E.-H. 1986, Ph.D. thesis. Univ. Texas at Austin